Engineering Structures 345 (2025) 121458

Contents lists available at ScienceDirect

Engineering Structures

journal homepage: www.elsevier.com/locate/engstruct

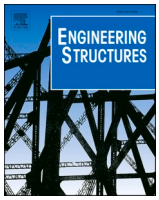

Nonlinear tension stiffening and cracking behaviour of concrete reinforced with EN 1.4301 and EN 1.4482 stainless steel rebars

H. Moodley [a,*], S. Afshan [a], P. Desnerck [b], J. Melo [c]

[a] Faculty of Engineering and Physical Sciences, University of Southampton, UK
[b] Department of Engineering, University of Cambridge, UK
[c] CONSTRUCT-LESE, Department of Civil Engineering, Faculty of Engineering, University of Porto, Portugal

ARTICLE INFO

Keywords:
Cracking width
Crack spacing
Codified crack width and spacing
Stainless steel rebar
Tension stiffening

ABSTRACT

This paper presents an experimental investigation into the tension stiffening behaviour and crack formation of concrete elements reinforced with stainless steel rebars. Specimens reinforced with 12 mm diameter cold-rolled austenitic EN 1.4301 and 16 mm diameter hot-rolled lean-duplex EN 1.4482 stainless steel rebars were tested under uniaxial tension, with strain and crack development monitored using a Digital Image Correlation (DIC) technique. The study compares the tension stiffening stress–strain responses and cracking behaviour of stainless steel and conventional B500C carbon steel rebars, showing broadly similar behaviour up to first cracking, but with differences emerging due to the nonlinear stress-strain response of stainless steel. In particular, stainless steel rebars exhibited a less pronounced tension stiffening effect in 12 mm bars, comparable behaviour in 16 mm bars and a continuation of tension stiffening beyond the 0.2 % proof stress that gradually decayed towards the bare rebar response. The applicability of codified models from *Eurocode 2*, *Model Code 1990* and *Model Code 2010*, including those for tension stiffening, crack spacing and crack width prediction, is assessed for stainless steel rebars. Finally, an improved tension stiffening model for stainless steel rebars is presented, based on *Model Code 1990*, *Model Code 2010* and *Eurocode* formulations and incorporating the Ramberg-Osgood stress-strain relationship.

1. Introduction

The durability of reinforced concrete structures is often compromised in aggressive environments, particularly those exposed to chloride ingress from marine atmospheres or de-icing salts. Corrosion of traditionally used carbon steel reinforcing bars (rebar) leads to deterioration mechanisms such as concrete cover spalling, bond degradation and loss of load-bearing capacity, ultimately reducing the service life of structures [1]. The economic, social and environmental costs associated with the maintenance and repair of corroding reinforced concrete infrastructure are substantial, with estimated expenditures reaching five billion euros per annum in Western Europe alone [2]. To address these costs, stainless steel rebars have gained attention as a corrosion-resistant alternative [3–5], while additionally offering advantageous mechanical properties such as high strength and ductility [6]. Recent examples of structures using stainless steel rebars in their construction include Stonecutters Bridge in Hong Kong and the Champlain Bridge in Montreal. Various life cycle cost (LCC) analysis studies have investigated the economic and carbon savings associated with using stainless steel rebar, with a comprehensive review provided in [7].

Understanding crack formation is critical for the design and performance assessment of reinforced concrete structures [8,9]. Crack widths and locations are primarily governed by the differential stress and strain distributions between the concrete and the steel reinforcement. The mechanical behaviour of stainless steel rebars differs from that of conventional carbon steel rebars. Unlike carbon steel, stainless steel exhibits a highly non-linear stress-strain response without a distinct yield point, combined with substantial strain hardening and superior ductility [6], [10–12]. These distinctive material properties directly influence the structural response of stainless steel reinforced concrete elements, particularly in relation to crack initiation, crack propagation and overall deformation behaviour. Since crack widths and deflections are key parameters in serviceability limit state design, a comprehensive understanding of crack formation and growth is required, both at the material level, through the tension stiffening effect, and at the structural level. Tension stiffening is a phenomenon where the bond between concrete

* Correspondence to: Department of Civil, Maritime and Environmental Engineering, University of Southampton, UK
E-mail address: h.t.m.moodley@soton.ac.uk (H. Moodley).

https://doi.org/10.1016/j.engstruct.2025.121458
Received 23 June 2025; Received in revised form 2 September 2025; Accepted 24 September 2025
Available online 1 October 2025

Table 1
Chemical compositions of stainless steel rebars from the mill certificates (%).

Steel Grade	C	Si	Mn	Cr	Mo	Cu	Ni	P	S	N	Ti
EN 1.4301-CR	0.057	0.400	1.580	18.07	0.300	0.470	8.010	0.036	0.001	0.060	0.005
EN 1.4482-HR	0.057	0.605	4.190	20.23	0.412	0.176	1.820	0.024	0.001	0.148	0.013

Table 2
Mill certificates tensile properties of tested stainless steel rebars.

Steel Grade	$R_{p,0.2}$ (MPa)	R_m (MPa)	A_{gt} (%)	A_5 (%)
EN 1.4301-CR	670	853	18	30
EN 1.4482-HR	581	815	32	42

and steel reinforcement allows the concrete between cracks to contribute to the overall stiffness of the member. Tension stiffening plays a critical role in controlling crack widths and influences the deformation characteristics of reinforced concrete structures. Accurately accounting for tension stiffening leads to more realistic modelling of reinforced concrete behaviour, especially in flexural members, where post-cracking stiffness significantly influences deflections and crack widths. Therefore, codified tension stiffening models are used to predict the tensile stress-strain response of reinforcing steel incorporating the concrete contribution.

This study aims to address this gap in literature through an experimental investigation on the tension stiffening behaviour of round ribbed stainless steel rebars. The experimental programme includes direct tension tests on two different stainless steel rebar types: 12 mm diameter cold-rolled austenitic EN 1.4301 and 16 mm diameter hot-rolled lean-duplex EN 1.4482, as well as control specimens using 12 mm and 16 mm B500C carbon steel rebars. Details of the experimental setup are described and the measured tension stiffening responses and crack behaviour using Digital Image Correlation (DIC) are presented and discussed. In addition, the applicability of the codified *Eurocode 2* [13], *Model Code 1990* [14] and *Model Code 2010* [15] tension stiffening models, crack width spacing and crack width analytical models to stainless steel rebars is assessed. An improved tension stiffening model for stainless steel rebars, based on *Model Code 1990*, *Model Code 2010* and *Eurocode 2* formulations and incorporating the Ramberg-Osgood stress-strain relationship, is developed. Finally, the main conclusions are outlined and suggestions for future research are proposed.

2. Experimental investigation

The tension stiffening tests were carried out in the Testing Structures Research Laboratory (TSRL) at the University of Southampton. Two stainless steel reinforcing bar materials were examined: 12 mm diameter cold-rolled austenitic EN 1.4301 (EN 1.4301-CR) and 16 mm diameter hot-rolled lean-duplex EN 1.4482 (EN 1.4482-HR). The chemical compositions and the mill certificate mechanical properties of the tested stainless steel rebars are presented in Table 1 and Table 2, respectively. The parameters in Table 2 are 0.2 % proof stress $R_{p,0.2}$, ultimate tensile stress R_m, total elongation at maximum force A_{gt} and elongation after fracture A_5. Carbon steel B500C rebars of the same diameters (12 mm and 16 mm) were included for comparison. The austenitic EN 1.4301 and lean-duplex EN 1.4482 grades, classified as Stainless Steel Resistance Class SSRC2 by *Eurocode 2* [13] based on their pitting resistance equivalent value, are considered suitable for most atmospheric and concrete cover environments. Lean duplex grades are a more cost-effective grade due to their lower initial material cost associated with reduced Ni alloying content (1.82 % compared to approximately 8 % in austenitic grades). The experimental setups for the material tests and the tension stiffening tests are described in this section.

2.1. Bare rebar tensile tests

Tensile tests were conducted to characterise the fundamental stress-strain behaviour of the bare rebars under monotonic tensile loading. All tests were performed using a 630 kN Schenck servo-hydraulic testing machine. The tensile specimens had an overall length of 400 mm, comprising 120 mm grip lengths with V-serrated hydraulic grips at each end and a 160 mm parallel length. Strain measurements were obtained using a clip-on extensometer with a 50 mm gauge length attached to the specimen. To verify the extensometer readings, a dot-tracking imaging method was also employed, utilising a Manta G504-B camera equipped with a Nikkor AF 50 mm f/1.8D lens, capturing images at 2 Hz. The acquired images were processed using the TrackMate [16] plug-in accessible in Fiji-ImageJ [17], enabling strain tracking between applied dots on the rebar. Additionally, to measure strain at fracture, initial gauge lengths of $L_o = 5.65\sqrt{A_o}$ were etched onto the ungripped section of the rebars, where A_0 is the rebar's cross-sectional area, taken as 113 mm^2 and 201 mm^2 for 12 mm and 16 mm diameter rebars, respectively. The tests were conducted under displacement control at a rate of 0.00025 strain/s, in accordance with *EN ISO 6892:2019* [18]. For each rebar specimen, two repeat tests were performed.(Fig. 1)

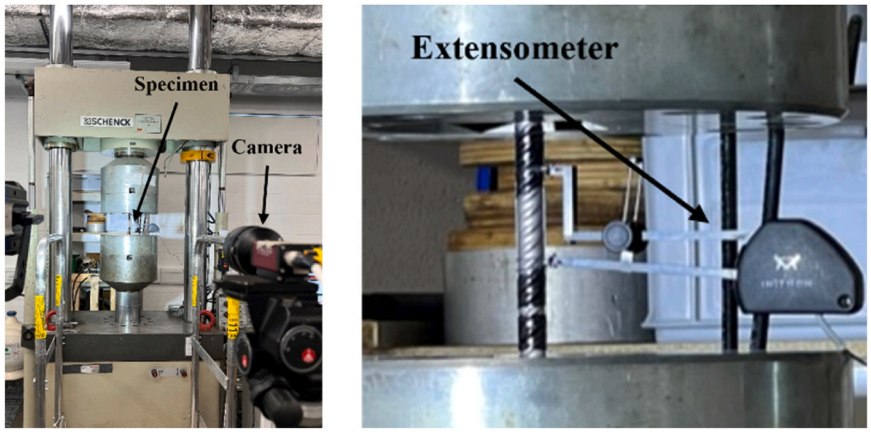

Fig. 1. Setup for bare rebar tensile tests.

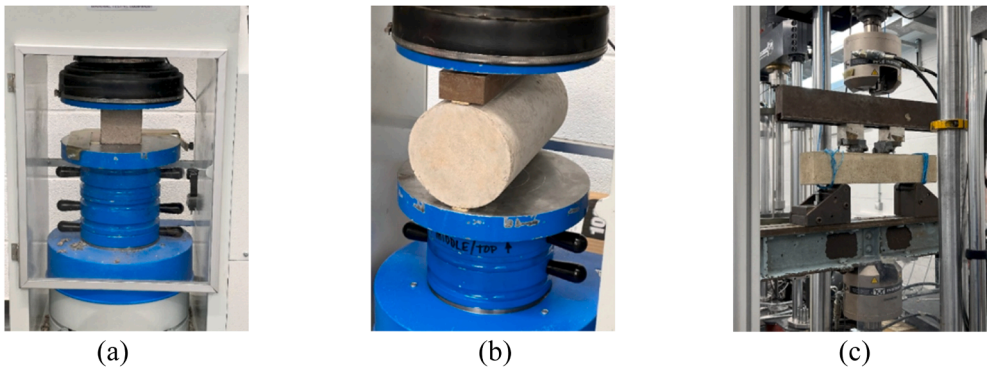

Fig. 2. Experimental setups for concrete compressive and tensile strengths. (a) Cube compression test. (b) Splitting tensile test. (c) Flexural strength test.

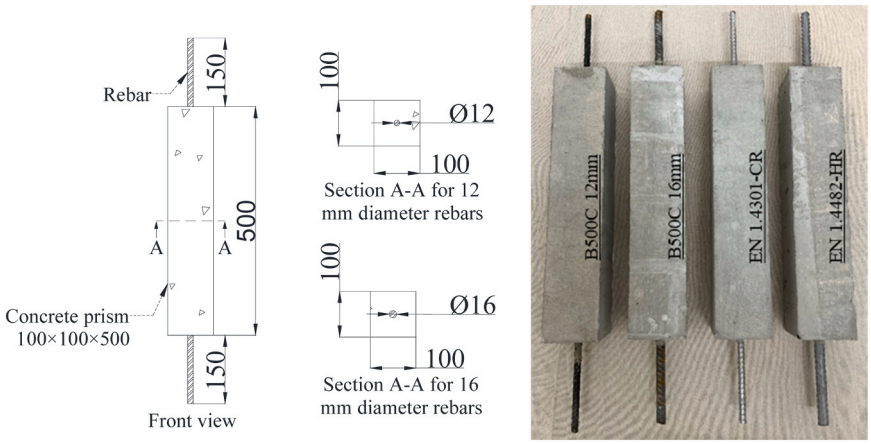

Fig. 3. Tension stiffening test specimens.

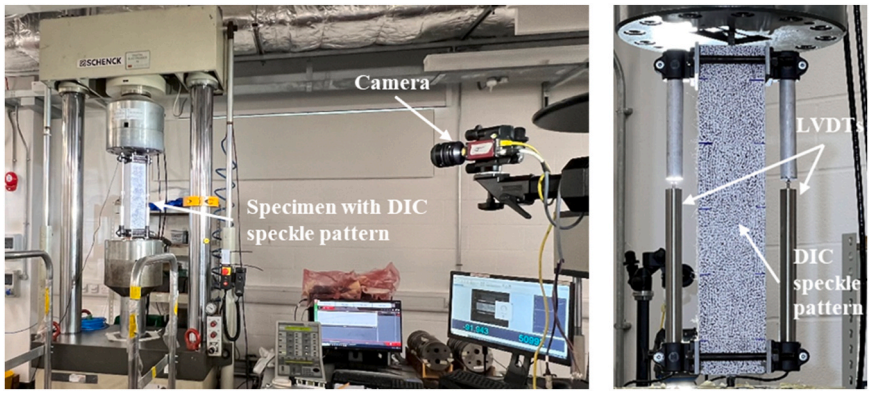

Fig. 4. Tension stiffening test setup and instrumentation.

2.2. Concrete tensile and compression tests

The compressive and tensile strengths of the concrete were measured using specimens made from the same concrete batch used to produce the tension stiffening specimens. Concrete cube tests on $100 \times 100 \times 100\ mm^3$ specimens were conducted to measure the 28-day cube compressive strength. The tests were performed in a UTEST testing machine under load control with a constant loading rate of 0.6 MPa/s in accordance with *EN 12390–3:2019* [19]. A total of 9 cube tests were performed, of which 8 exhibited the correct failure mode and were used to obtain the average cube compressive strength.

Two test methodologies were used to obtain the tensile strength of the concrete at 28 days, which included splitting tensile test and flexural strength test. Cylindrical concrete specimens (150 mm diameter and 300 mm height) were used for the splitting tensile tests. The tests were performed using the UTEST testing machine. The cylinder specimens were placed horizontally in the test machine and load was applied over the full length of the upper side of the cylinder specimen through a rectangular loading block. The applied compressive load induces tensile stresses along the plane of the load application, causing the specimen to fail in tension with a split across the centre of the cross-section. The load was applied at a rate of 0.7 MPa/min in accordance with *ASTM C496/C496M-04* [20]. A total of 6 splitting tensile tests were conducted. In addition, a total of 3 flexural strength tests were carried out on square cross-section prism specimens with 100 mm× 100 mm× 500 mm dimensions. The specimens were tested under a four-point bending

Table 3
Specifications and parameters for 2D DIC.

2D DIC	
Camera	
Sensor & Digitalisation	CCD 2456 × 2058 pixels, 8-bit
Exposure time & recording rate	15,000 μs, 3 Hz
Lens & imaging distance	Nikkor AF 28 mm, 2.00 m
Number of images averaged for resolution calculations	2
Pixel size	3.45 μm
Processing	
Subset, step	29, 8 pixels
Matching criterion, interpolation, shape function	ZNSSD, Local Bicubic Spline, Affine
Prefiltering	Gaussian
Strain	
Smoothing technique	None
Virtual strain gauge	7 pixels (24.15 μm)
Noise evaluation	
Mean camera noise	0.90 %
Noise floor horizontal displacement	0.017 mm
Noise floor vertical displacement	0.015 mm

arrangement using an Instron 8802 100 kN servo-hydraulic testing machine. The two loading points and end supports were symmetrically positioned at 50 mm and 150 mm from the centreline of the specimen, respectively. Loading was applied at a rate of 4 kN/min, in accordance with *ASTM C78/78M-18* [21], until failure.(Fig. 2)

2.3. Tension stiffening tests

A total of twelve tension stiffening specimens were cast, with three repeat specimens for each type of reinforcing steel to account for the inherent randomness of cracking. Each specimen was a 100 mm× 100 mm× 500 mm concrete prism, centrally encasing an 800 mm long rebar over its central 500 mm length consistent with similar literature tests [8,22]. The concrete covers were 44 mm and 42 mm for the tension stiffening specimens containing 12 mm and 16 mm diameter rebars, respectively. Hence, the concrete cover-to-bar diameter ratio for both cases exceeded 2.5, which is above the minimum requirement specified in *Eurocode 2* [13] for adequate bond force transmission (equal to the bar diameter). The remaining 150 mm of rebar extending from both ends was required for gripping the specimens inside the test machine. The dimensions and configurations of the test specimens are shown in Fig. 3. It should be noted that the influence of concrete shrinkage and creep was not considered in this study, as all tests were performed under short-term monotonic loading. The specimens were tested in the same 630 kN Schenck servo-hydraulic testing machine as for the bare rebar tensile tests, under the same strain rate of 0.00025 strain/s, using the setup shown in Fig. 4. The rebars were gripped at each end over a 120 mm length. The mean strain was measured over the central 450 mm length of the concrete prism using the average reading of two LVDTs mounted on either side of the concrete prism. Two-dimensional Digital Image Correlation (DIC) was employed to monitor the crack development, width and spacing throughout testing. Images for the DIC were taken using a Manta G-504B camera with a Nikkor AF 28 mm lens at a frame rate of 3 Hz, and images were processed using MatchID 2D software. The camera, settings, parameters and noise evaluation used in DIC are reported in Table 3.

3. Experimental results

3.1. Rebar material properties

The tensile stress-strain responses of the stainless steel and carbon steel rebars are shown in Fig. 5. Carbon steel rebars exhibit a linear elastic response up to the yield point, followed by a distinct yield plateau, after which strain hardening occurs before final fracture. In

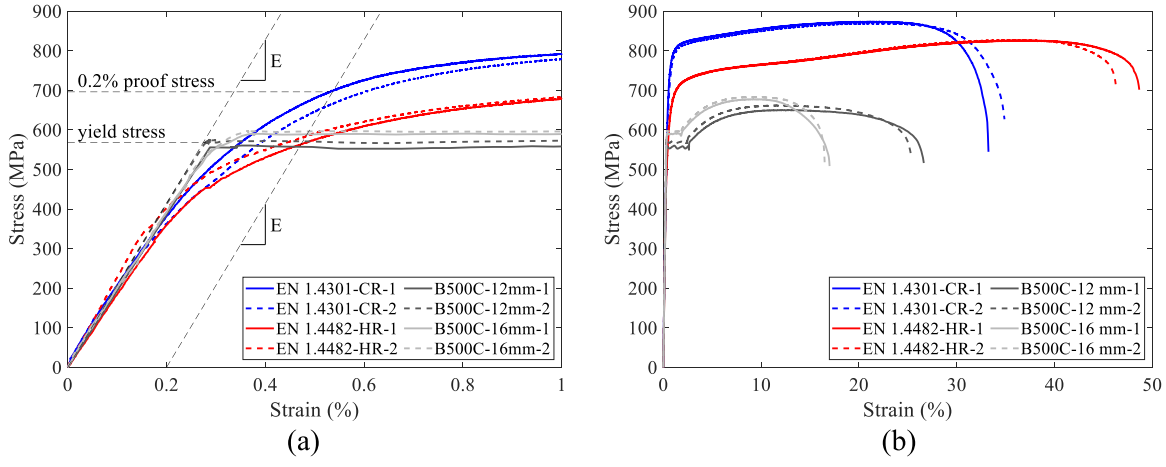

Fig. 5. Measured tensile stress-strain responses of bare rebars.(a) 0% - 1% strain. (b) 0% - 50% strain.

Table 4
Key measured rebar tensile parameters.

Specimen	E (N/mm²)	f_y (N/mm²)	f_u (N/mm²)	ε_u (%)	$\varepsilon_{f,pl}$ (%)	n	n'
EN 1.4301-CR−1	205,000	696	874	22.1	34.2	4.43	6.76
EN 1.4301-CR−2	210,000	658	870	21.4	35.8	3.58	7.39
EN 1.4482-HR−1	190,000	576	826	36.7	43.8	6.18	4.97
EN 1.4482-HR−2	210,000	581	828	35.7	46.8	7.68	4.77
B500C−12mm−1	207,000	567	663	10.2	-	-	-
B500C−12mm−2	193,000	553	651	12.6	-	-	-
B500C−16mm−1	195,000	591	679	8.85	-	-	-
B500C−16mm−2	196,000	597	684	8.48	-	-	-

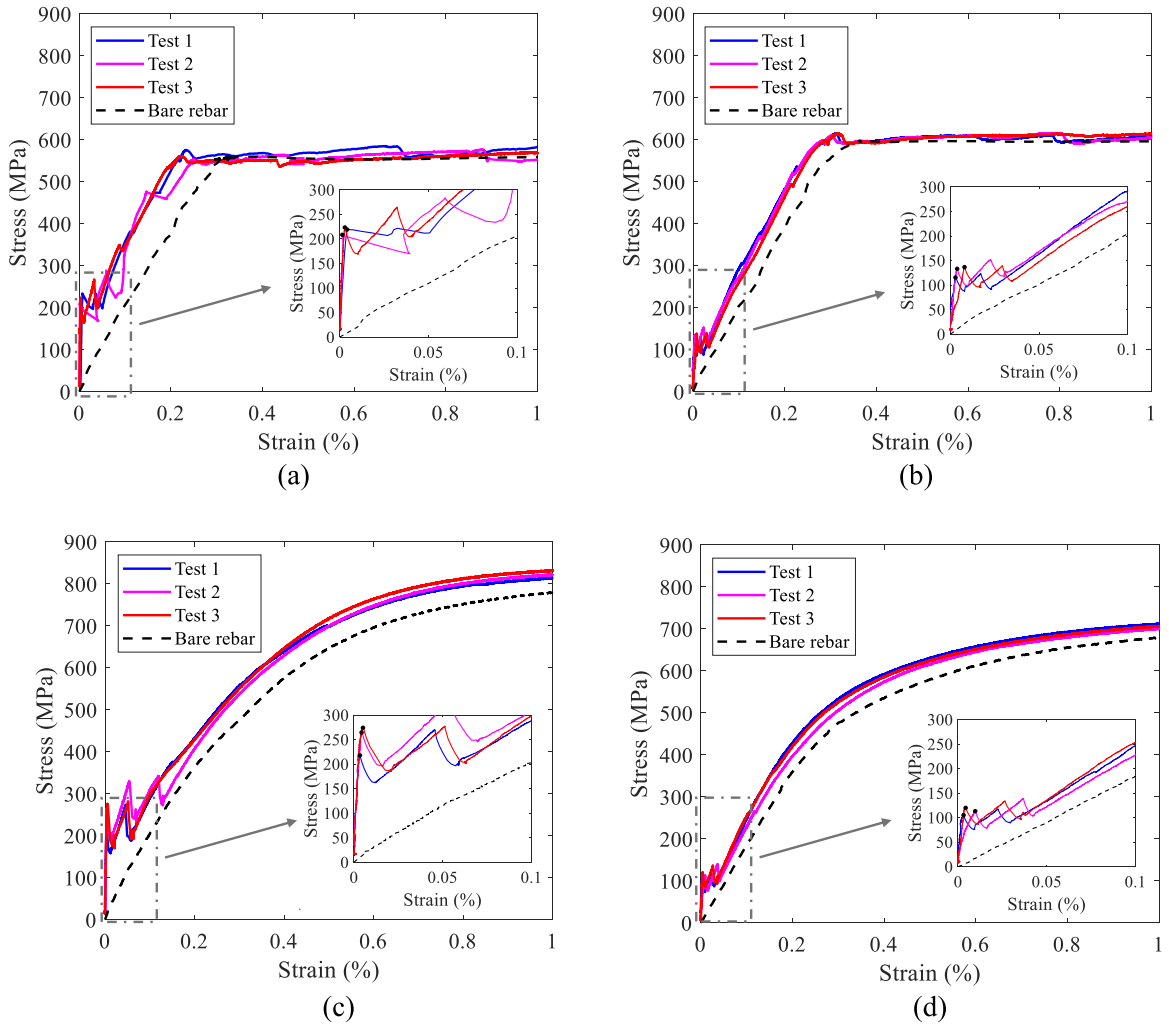

Fig. 6. Tension stiffening responses of carbon and stainless steel specimens.(a) B500C 12mm. (b) B500C 16mm. (c) EN 1.4301-CR 12mm. (d) EN 1.4482-HR 16mm.

Table 5
Summary of measured tension stiffening parameters (values based on average of three repeat tests per rebar material).

Specimen	$E_{initial}$ (N/mm2)	σ_{cr} (N/mm2)	(ε_{rebar} - ε_{TS}) (%)	$E_{initial}$/E	$\sigma_{cr,16}$/$\sigma_{cr,12}$	$\sigma_{cr,ss}$/$\sigma_{cr,cs}$
1.4301-CR−12mm	6686,000	253.4	0.060	32.2	-	1.13
1.4482-HR−16mm	2532,000	113.2	0.045	12.7	0.45	0.88
B500C−12mm	7651,000	223.0	0.082	38.3	-	-
B500C−16mm	2401,000	129.4	0.041	12.3	0.58	-

contrast, stainless steel rebars display a highly nonlinear response from the outset, lacking a well-defined yield point while exhibiting greater ductility, pronounced strain hardening and a higher yield-to-ultimate strength ratio. The key measured tensile properties are summarised in Table 4, where E is the Young's modulus, f_y is the yield strength (taken as the 0.2 % offset strength $f_{0.2}$ for stainless steel), f_u is the ultimate tensile strength, ε_u is the strain at ultimate tensile strength, and $\varepsilon_{f,pl}$ is the plastic strain at fracture. Moreover, parameters n and n' of the Ramberg-Osgood model [23,24], which is commonly used to model the stress-strain behaviour of stainless steels, derived using the fitting method from Afshan et al. [25], are presented in Table 4.

3.2. Concrete material properties

The mean measured 28-day compressive cube strength, $f_{c,cube100}$, of the eight specimens was 63.58 MPa with a coefficient of variation (COV) of 6.89 %. The $f_{c,cube100}$ values were converted to equivalent 150 mm diameter cylinder strengths, $f_{c,cylinder}$, using Eq. (1), proposed by L'Hermite [26], resulting in a mean cylinder strength $f_{c,cylinder}$ of 52.4 MPa. The measured 28-day mean tensile strength, f_t, obtained from splitting tension tests was 3.70 MPa with a COV of 8.7 %, while the flexural tests produced a mean tensile strength of 3.75 MPa with a COV of 17.3 %.

$$f_{c,cylinder} = \left[0.76 + 0.2\log_{10}\left(0.96f_{cube,100}\Big/19.6\right)0.96f_{cube,100}\right] \quad (1)$$

3.3. Tension stiffening stress-strain response

The measured stress-strain responses of the stainless and carbon steel rebar tension stiffening tests are presented in Fig. 6. Strain was determined as the change in length measured by each of the LVDTs divided by the original 450 mm gauge length, and stress was calculated as the force measured by the machine load cell divided by the rebar cross-sectional area. The mean strain from the two LVDTs was used to plot the stress-strain responses shown in Fig. 6. Additionally, the stress-strain responses of the corresponding bare rebars are also depicted for comparison. Compared to the bare rebar tensile stress-strain responses, the rebars encased in concrete exhibits higher initial linear stiffness, as

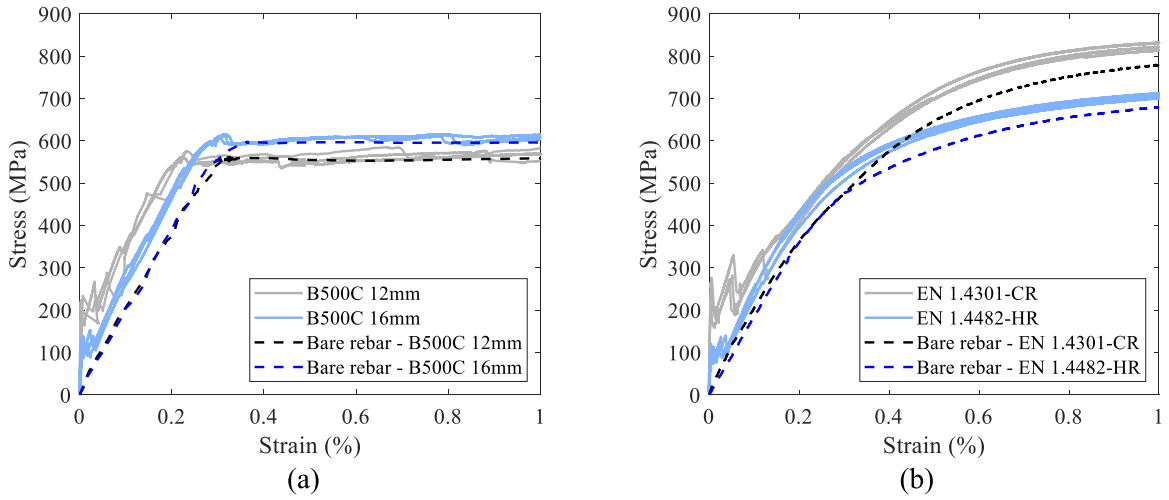

Fig. 7. Comparisons of the tension stiffening responses of 12 mm and 16 mm diameter rebars.(a) Carbon steel rebars. (b) Stainless steel rebars.

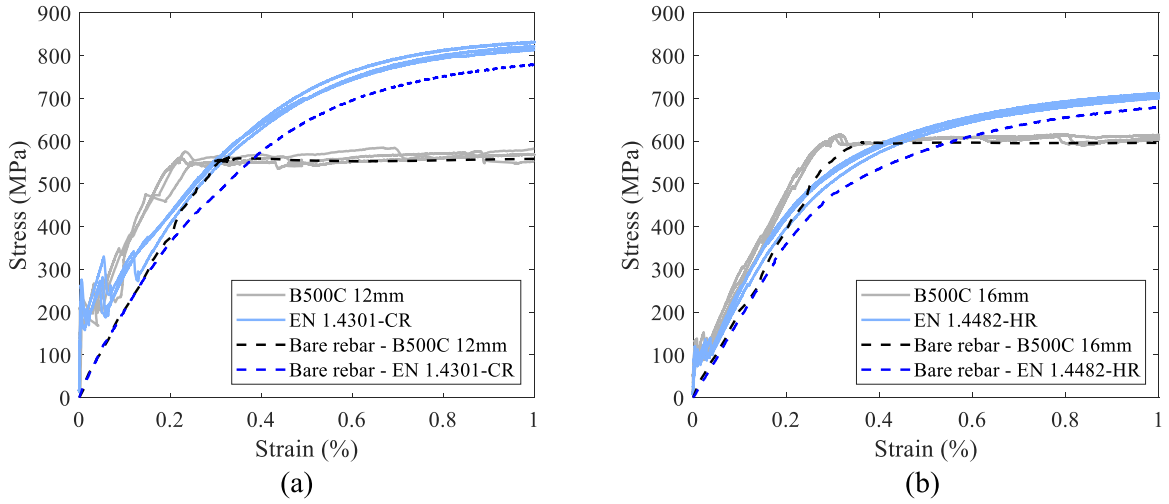

Fig. 8. Comparisons of the tension stiffening responses of specimens with stainless steel and carbon steel rebars.(a) 12 mm diameter rebars. (b) 16 mm diameter rebars.

indicated by the ratios of initial stiffness $E_{initial}$ to rebar stiffness E presented in Table 5. This increase is observed up to the formation of the first crack at the cracking rebar stress σ_{cr}, due to the concrete's contribution in resisting tensile load. The cracking of the concrete is observed in the stress-strain responses as sudden drops in stress. After the first crack, further cracks continue to form as the applied load increases, causing stiffness degradation after every crack until the final crack forms and the primary crack pattern along the specimen is established. Finally, a stable post-cracking stage is reached, where the stress-strain response follows a path parallel to that of the bare rebar until the rebar reaches yield, with the post-yield stage approaching that of the bare rebar.

The reinforcement ratio was found to impact the tension stiffening stress-strain responses. Fig. 7a and b show the tension stiffening responses of carbon and stainless steel 12 mm and 16 mm diameter rebars, with reinforcement ratios $A_s/A_c = 1.14$ % and 2.05 %, respectively, where A_s and A_c are the steel and concrete cross-sectional areas. The results show that for both rebar materials, the cracking stress was lower for the 16 mm rebars compared to the 12 mm rebars as shown by the ratios of $\sigma_{cr,16}/\sigma_{cr,12}$ presented in Table 5. This is expected due to the larger rebar cross-sectional area and the reduced concrete cover of the 16 mm rebars, both contributing to a lower cracking stress. Furthermore, for both rebar materials, the tension stiffening response of the 16 mm diameter rebars in the post-cracking stable stage was closer to that of the corresponding bare rebar than for the 12 mm diameter rebars, as indicated by the difference between the rebar strain and the tension stiffening strain ($\varepsilon_{rebar} - \varepsilon_{TS}$), calculated as the average in the stress range of $0.5f_y$ to $0.9f_y$, as reported in Table 5.

Comparisons of the tension stiffening behaviour of EN 1.4301-CR and EN 1.4482-HR stainless steel rebars with corresponding diameter B500C carbon steel rebars are presented in Fig. 8. The tension stiffening responses of the stainless steel and carbon steel rebars show similar linear stages up to the first crack and crack formation stages. However, the cracking stress of the 12 mm diameter stainless steel rebars was slightly greater than that of the corresponding 12 mm carbon steel rebars ($\sigma_{cr,ss}/\sigma_{cr,cs} = 1.13$), while for 16 mm rebars carbon steels had slightly higher value ($\sigma_{cr,ss}/\sigma_{cr,cs} = 0.88$). The greatest difference between the tension stiffening responses of stainless and carbon steel rebars is in the shape of their post-cracking stable stage, where the tension stiffening responses show similar shapes to their respective bare rebars i.e., linear with a yield plateau for carbon steel and nonlinear with no distinct yield point for stainless steel [10,11].

The 12 mm stainless steel tension stiffening response in the stable post-cracking stage is closer to that of the bare rebar, compared to the 12 mm carbon steel rebar. This suggests that the so-called tension stiffening effect, i.e., the difference in strain between the tension stiffening and bare rebar responses ($\varepsilon_{rebar} - \varepsilon_{TS}$), as reported in Table 5, is

Fig. 9. DIC images of crack patterns of tension stiffening responses at rebar yield stress.

Table 6
Measured crack spacing (mm) from DIC.

	B500C 12 mm	B500C 16 mm	EN 1.4301-CR	EN 1.4482-HR
Test 1	157.50	148.01	165.19	173.96
Test 2	95.91/80.40	213.75	143.96/110.12	180.73
Test 3	139.66	165.24	165.31	147.36
Average	118.37	175.67	146.15	167.35
COV (%)	30.5	19.4	17.8	10.5

less for the 12 mm diameter stainless steel rebar. However, there was no noticeable difference in the tension stiffening effect between the 16 mm diameter stainless and carbon steel rebars. Furthermore, the effect of tension stiffening effect in stainless steel rebar specimens continues beyond the yield stress point (0.2 % proof stress), as shown in Fig. 8, where it gradually begins to decay, with the stress-strain response becoming asymptotic to the bare rebar tensile response beyond this point. This behaviour may potentially impact the deflections and crack widths of stainless steel reinforced concrete members beyond yield.

3.4. Tension stiffening crack spacing

Although the primary focus of this study was on tension stiffening behaviour, the recorded crack measurements also enabled an examination of crack spacing and width; while such characteristics are more commonly derived from beam tests, they were assessed here using tension stiffening specimens. The crack patterns, measured using DIC, at the stress corresponding to the rebar yield stress, taken as the 0.2 % proof stress for the stainless steel rebars, are shown in Fig. 9. All tension stiffening specimens developed two transverse cracks during the cracking stage of the tension stiffening response, except for Test 2 of both the B500C 12 mm and EN 1.4301-CR specimens, which developed three transverse cracks. The measured crack spacings at the stress corresponding to the rebar yield stress, obtained from the DIC results, are

Table 7
Measured mean crack widths (mm) for carbon steel rebar specimens.

Test/Stress point	B500C 12 mm				B500C 16 mm			
	0.5 f_y	f_y	1.05 f_y	1.1 f_y	0.5 f_y	f_y	1.05 f_y	1.1 f_y
Test 1	0.15	0.56	3.05	6.51	0.20	0.49	3.21	5.12
Test 2	0.18	0.34	1.73	4.19	0.39	0.66	4.52	7.10
Test 3	0.36	0.50	4.03	6.74	0.37	0.63	3.85	5.21
Average	0.23	0.47	2.94	5.81	0.32	0.60	3.86	5.81
COV (%)	49.4	24.4	39.3	24.3	32.6	15.3	17.0	19.2

Table 8
Measured mean crack widths (mm) for stainless steel rebar specimens.

Test/Stress point	EN 1.4301-CR				EN 1.4482-HR			
	0.5 f_y	f_y	1.05 f_y	1.1 f_y	0.5 f_y	f_y	1.05 f_y	1.1 f_y
Test 1	0.29	0.94	1.02	1.12	0.31	0.88	1.02	1.20
Test 2	0.24	0.59	0.66	0.74	0.26	0.84	0.99	1.19
Test 3	0.34	0.99	1.10	1.22	0.30	0.91	1.06	1.24
Average	0.29	0.84	0.93	1.03	0.29	0.88	1.02	1.21
COV (%)	17.2	26.0	25.3	24.7	9.1	4.0	3.4	2.2

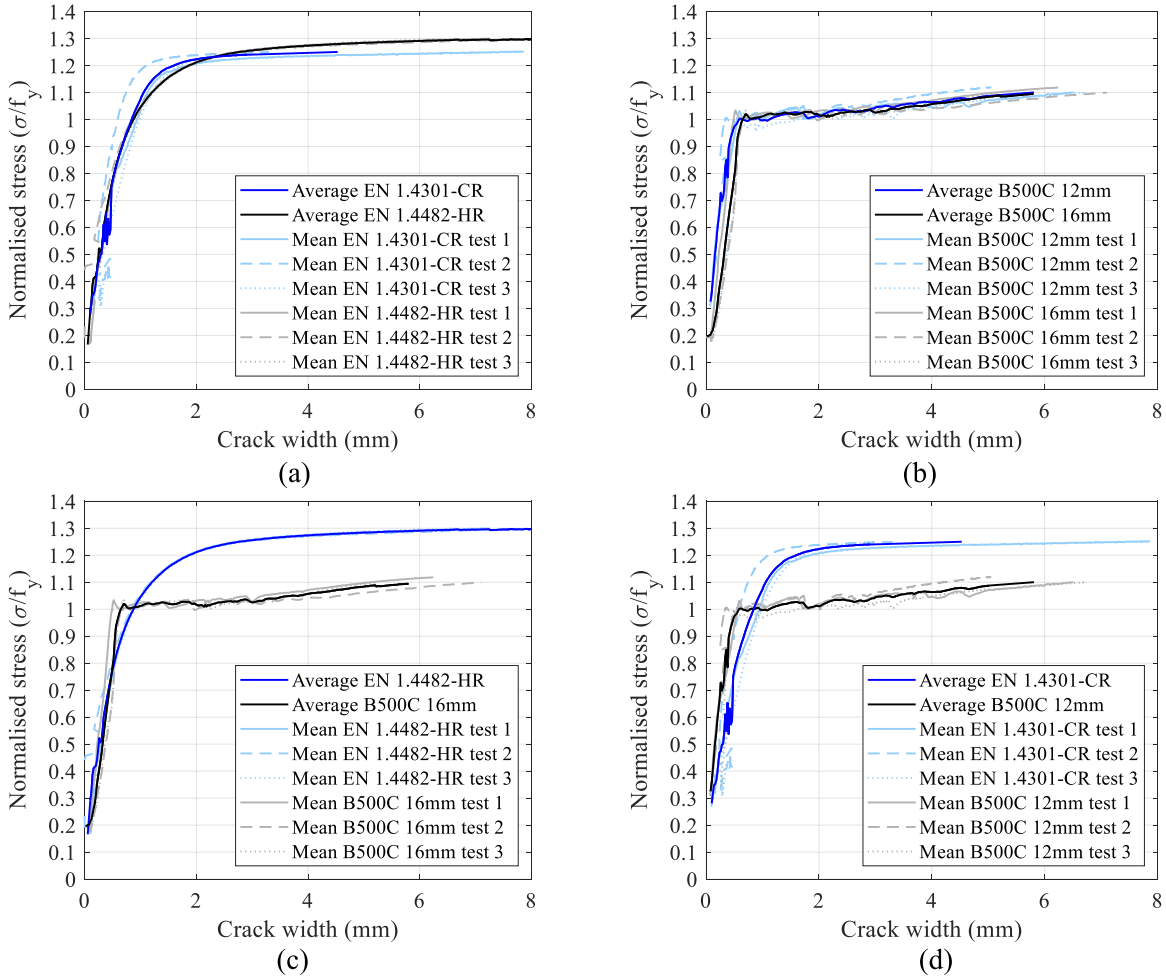

Fig. 10. Comparisons of measured crack widths for stainless steel and carbon steel rebar specimens.(a) EN 1.4301-CR vs. EN 1.4482-HR. (b) B500C 12mm vs. B500C 16mm. (c) EN 1.4482-HR vs. B500C 16mm. (d) EN 1.4301-CR vs. B500C 12mm.

reported in Table 6, where the average and COV values are also included. The average measured crack spacing in specimens containing 16 mm rebars were larger than those containing 12 mm rebars, for both carbon and stainless steels. According to the transmission length relationship, i.e., the minimum distance from an existing crack where another crack can form $l_{s,max}$ from *Model Code 1990* [14], given by Eq. (2), crack spacing is directly related to the concrete tensile strength f_t and rebar diameter $\emptyset$, and inversely related to the bond strength τ_{bm} and

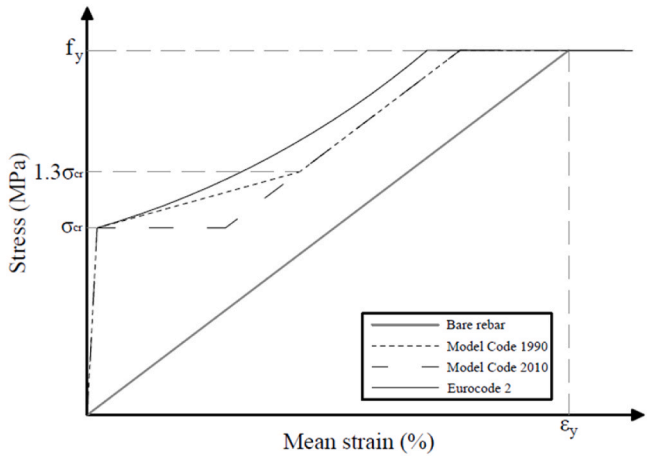

Fig. 11. Schematic of codified tension stiffening model.

reinforcement ratio ρ_s (=A_s/A_c). Hence, the larger measured average crack spacing in EN 1.4301-CR specimens compared to B500C 12 mm carbon steel specimens can be attributed to the comparatively lower bond strength of cold-rolled austenitic EN 1.4301 rebars, as observed in the study by [27].

$$l_{s,max} = (f_t/4\tau_{bm})(\varnothing/\rho_s) \quad (2)$$

3.5. Tension stiffening crack width

The crack widths were also determined from the DIC measurements. For each specimen, where two or three cracks were developed, the mean crack width, which refers to the average of the crack widths across multiple cracks in a given specimen, were considered. The mean crack widths at stresses corresponding to $0.5f_y$, f_y, $1.05f_y$ and $1.1f_y$, where f_y is the rebar yield stress, are reported in Tables 7 and 8 for carbon and stainless steel rebar specimens, respectively. The average values across three repeat tests and corresponding COV values are also reported.

The measured crack widths of the different tension stiffening specimens are compared in Fig. 10, where the development of crack width over the applied rebar stress range, normalised by the rebar yield stress, is plotted. For each rebar size and grade, the mean crack widths for each specimen, as well as the average crack width from three repeated tests, are shown. The normalised stress and mean crack width responses shown in Fig. 10 exhibit similar behaviour to the stress-strain of their corresponding rebars. For specimens reinforced with stainless steel rebar, the response is nonlinear, lacking a distinct yield point, as shown in Fig. 10a. In contrast, specimens with carbon steel rebar exhibit a more linear response up to yield, followed by a yield plateau and subsequent hardening, as shown in Fig. 10b.

The responses shown in Fig. 10c indicate that the mean crack widths of the 16 mm carbon and stainless steel specimens are comparable up to a stress value of $0.5f_y$. As the stress increases from $0.5f_y$ to f_y, the difference in the mean crack widths between stainless steel and carbon steel rebars becomes more pronounced. At stress equal to f_y, the average crack width of the carbon steel rebar specimens is 38 % smaller than that of the stainless steel tension stiffening specimens. For the specimens with 12 mm rebars, shown in Fig. 10d, the mean crack width of the carbon steel specimens is smaller than those of the stainless steel specimens across the entire stress range up to f_y, where a 39 % difference in the average crack width curves is observed. The mean crack width can be estimated as the product of crack spacing and the difference in strain between the steel rebar and concrete. Hence, the larger crack widths of the 12 mm EN 1.4301-CR rebars at stresses $\leq f_y$ are attributed to their greater crack spacing (indicating poorer bond strength) and higher strain at the yield point compared to 12 mm carbon steel rebars. Similarly, the larger mean crack widths of the 16 mm EN 1.4482-HR rebars at stresses $\leq f_y$ are primarily due to their higher strain at yield compared with 16 mm carbon steel rebars.

Beyond yield, the crack widths of specimens reinforced with carbon steel rebars increase rapidly relative to those reinforced with stainless steel rebars, as shown in Fig. 10c and d. At $1.05f_y$, the average of the mean crack widths of the carbon steel rebars are 216 % and 268 % greater than the specimens reinforced with 12 mm and 16 mm stainless steel rebars, respectively. This gap widens further as stress reaches $1.1f_y$. The divergence in post-yield crack width behaviour is attributed to differences in the stress-strain characteristics of the two materials. Stainless steel rebars lack a yield plateau, exhibit earlier and greater post-yield strain hardening, and the tension stiffening effect continues post-yield. As a result, the strains corresponding to $1.05f_y$ and $1.1f_y$ in stainless steel reinforced specimens are lower than the corresponding strains in carbon steel reinforced specimens. Consequently, the smaller post-yield crack widths in stainless steel reinforced specimens are due to their post-yield behaviour under the same stress levels.

4. Assessment of codified tension stiffening, crack spacing and width models

4.1. Assessment of codified tension stiffening models

4.1.1. Overview of codified tension stiffening stress-strain models

Analytical stress-strain models have been developed to predict the tension stiffening behaviour of reinforced concrete structures. Three such models, provided by the *Model Code 1990* [14], *Model Code 2010* [15] and *Eurocode 2* [13] were investigated in this paper. The models from *Model Code 1990* and *Model Code 2010* follow a four-stage approach, whereas the *Eurocode 2* model consists of three-stages, schematics of which are shown in Fig. 11. All models begin with the same linear stress-strain relationship during the initial uncracked stage, up to the cracking stress σ_{cr}, where the first crack forms. In this stage, it is assumed that the concrete and steel experience equal strains, referred to as the mean strain, ε_m, as they jointly resist the total force F, as expressed in Eq. (3), where E_c and E are concrete and steel elastic modulus and A_c and A_s are the concrete and steel cross-sectional areas, respectively. The cracking stress σ_{cr} is reached when the concrete first attains its tensile strength f_t, as given by Eq. (4), where all parameters are as previously defined, with ρ_s and α_s representing the ratios of steel to concrete cross-sectional area and steel to concrete elastic modulus, respectively.

$$F = F_{concrete} + F_{steel} = \varepsilon_m E_c A_c + \varepsilon_m E A_s \quad (3)$$

$$\sigma_{cr} = f_t A_c (1 + \alpha_s \rho_s)/A_s \quad (4)$$

Beyond the first cracking point, the three models adopt different stress-strain relationships for the crack formation and stabilisation stages. The *Model Code 1990* uses a bi-linear stress-strain relationship, where the stress increases from the initial cracking stress σ_{cr} to the final cracking stress, taken as $1.3\sigma_{cr}$, during the crack formation stage. After this, the stress-strain response follows the same stiffness as the bare rebar during the crack stabilisation stage, continuing up to the yield stress f_y of the rebar. The assumption that crack formation occurs between σ_{cr} and $1.3\sigma_{cr}$ accounts for the inherent scatter in the tensile strength of concrete, leading to cracks forming at progressively higher loads beyond the initial cracking load. The stress σ and mean strain ε_m relationships for the crack formation and crack stabilisation stages are given by Eqs. (5) and (6), respectively.

$$\varepsilon_m = \varepsilon_2 - \frac{\beta_t(\sigma - \sigma_{cr})(1.3\sigma_{cr} - \sigma)}{(1.3\sigma_{cr} - \sigma_{cr})}(\varepsilon_{sr,2} - \varepsilon_{sr,1}) \quad \text{for} \quad \sigma_{cr} < \sigma \leq 1.3\sigma_{cr} \quad (5)$$

$$\varepsilon_m = \varepsilon_2 - \beta_t(\varepsilon_{sr,2} - \varepsilon_{sr,1}) \quad \text{for} \quad 1.3\sigma_{cr} < \sigma \leq f_y \quad (6)$$

where, ε_2 is the strain in the fully cracked state i.e., the bare rebar (ε_2 =

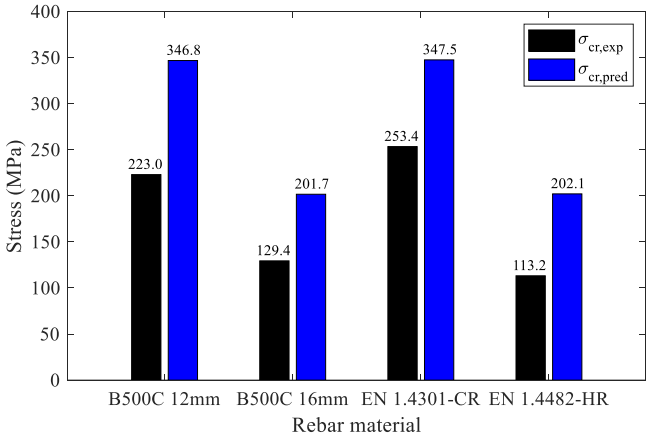

Fig. 12. Comparisons of predicted and measured cracking stresses.

σ/E), β_t is a coefficient related to the duration of loading, taken as 0.4 for short term loading, $\varepsilon_{sr,2}$ is the steel strain when the first crack occurs ($\varepsilon_{sr,2} = \sigma_{cr}/E$) and $\varepsilon_{sr,1}$ is the steel strain at the point of zero slip at the occurrence of the initial crack ($\varepsilon_{sr,1} = F_{cr}/(E_cA_c + EA_s)$).

The *Model Code 2010* simplifies the crack formation stage to a stress plateau equal to the cracking stress σ_{cr} up to a mean strain interception point $\varepsilon_{m,int}$ as given by Eq. (7). Beyond this point, a linear stress-strain relationship with the same stiffness as the bare rebar is assumed over the crack stabilisation stage, as described by Eq. (8).

$$\varepsilon_{m,int} = \frac{0.6f_t}{E\rho_s} \tag{7}$$

$$\varepsilon_m = \varepsilon_2 - 0.4\frac{f_t}{E\rho_s} \quad \text{for} \quad \varepsilon_m > \varepsilon_{m,int} \text{ and } \sigma_{cr} < \sigma \leq f_y \tag{8}$$

The *Eurocode 2* model assumes a nonlinear ascending stress-strain relationship in the stress range from σ_{cr} to f_y, as given by Eq. (9). In this equation, ε_1 is the strain of the uncracked section at the assessed force ($\varepsilon_1 = F/(E_cA_c + EA_s)$) and ζ is a distribution or tension stiffening coefficient, which can be calculated using Eq. (10), where β_1 is a coefficient accounting for the duration of loading, taken as 1 for single short-

Table 9
Comparisons of codified model and measured (value based on average of three repeat tests per rebar material) dissipated energy of tension stiffening responses up to the at yield stress of the bare rebar.

	B500C 12 mm	B500C 16 mm	EN 1.4301-CR	EN 1.4482-HR
Test (MPa)	0.871	1.163	2.019	1.469
Eurocode 2 (MPa)	0.863	1.101	2.389	1.563
Model Code 1990 (MPa)	0.812	1.101	2.322	1.569
Model Code 2010 (MPa)	0.790	1.094	2.296	1.564
Test/Eurocode 2	1.008	1.056	0.845	0.940
Test/Model Code 1990	1.072	1.056	0.869	0.939
Test/Model Code 2010	1.102	1.063	0.879	0.936

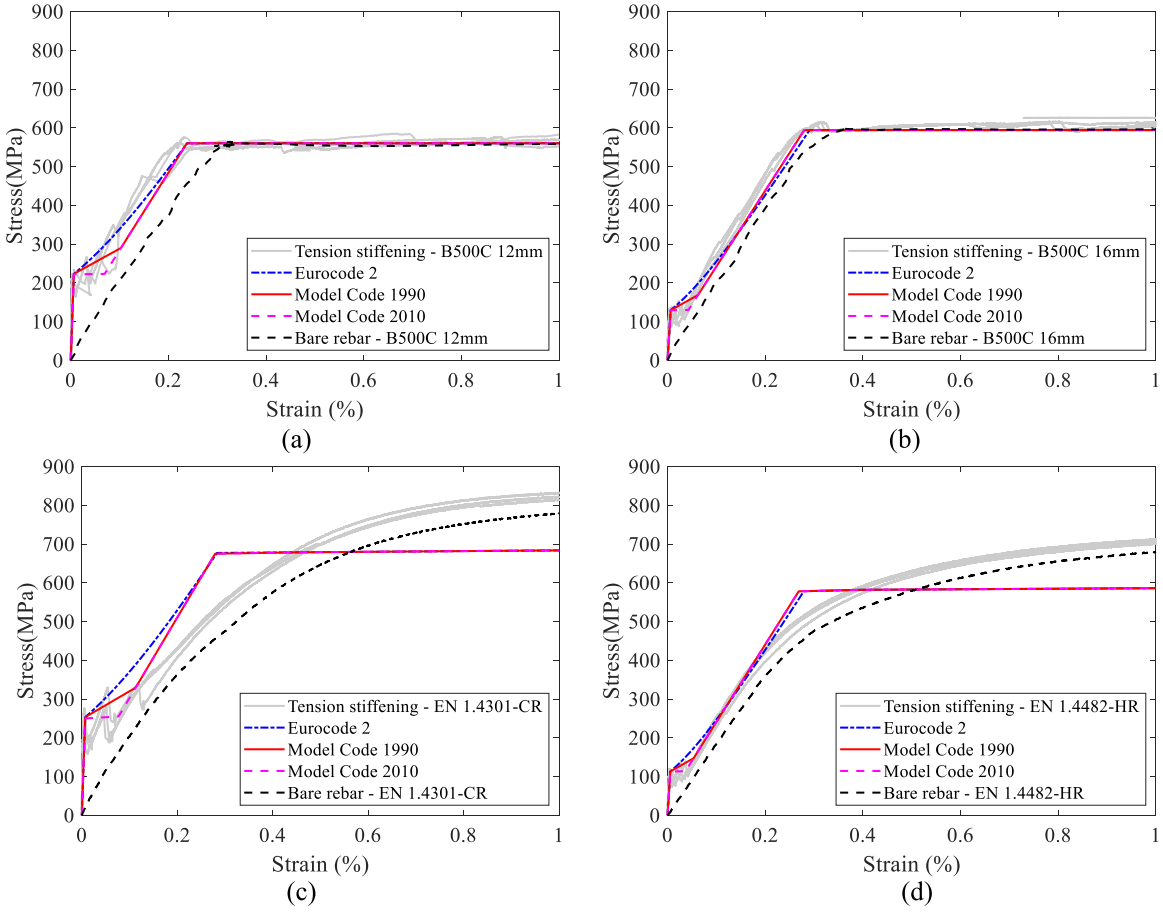

Fig. 13. Comparison of predicted and measured tension stiffening stress-strain responses using experimental cracking stress $\sigma_{cr,exp}$. (a) B500C 12mm. (b) B500C 16mm. (c) EN 1.4301-CR 12mm. (d)EN 1.4482-HR 16mm.

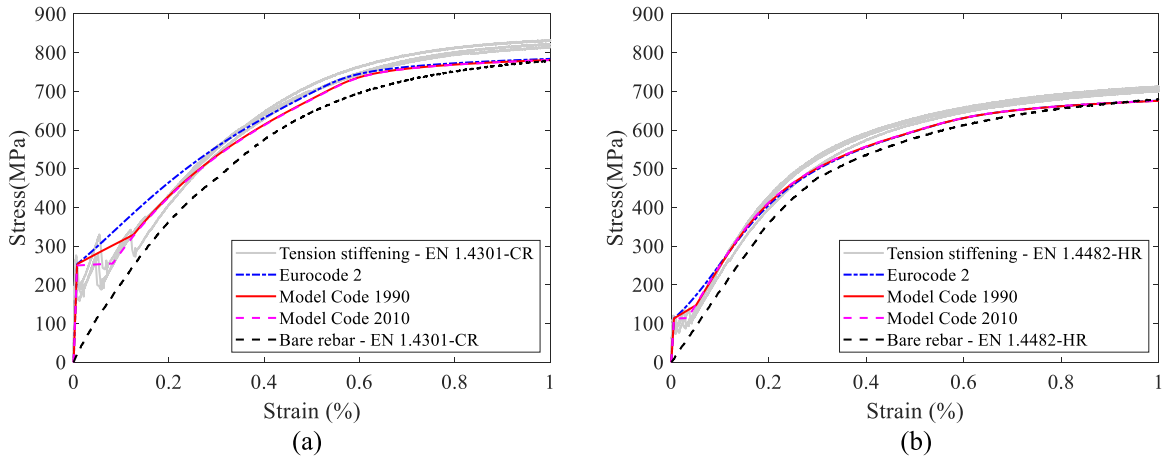

Fig. 14. Comparison of modified model predicted and measured tension stiffening stress-strain responses for stainless steel rebars using experimental cracking stress $\sigma_{cr,exp}$.(a) EN 1.4301-CR. (b) EN 1.4482-HR.

Table 10
Comparison of modified codified models and average measured (average of three repeat tests per rebar material) dissipated energy of stainless steel tension stiffening responses up to yield stress of bare rebar.

	EN 1.4301-CR	EN 1.4482-HR
Test (MPa)	2.019	1.469
Modified Eurocode 2 (MPa)	2.138	1.450
Modified Model Code 1990 (MPa)	1.982	1.446
Modified Model Code 2010 (MPa)	1.960	1.440
Test/Modified Eurocode2	0.944	1.012
Test/Modified Model Code 1990	1.019	1.015
Test/Modified Model Code 2010	1.030	1.019

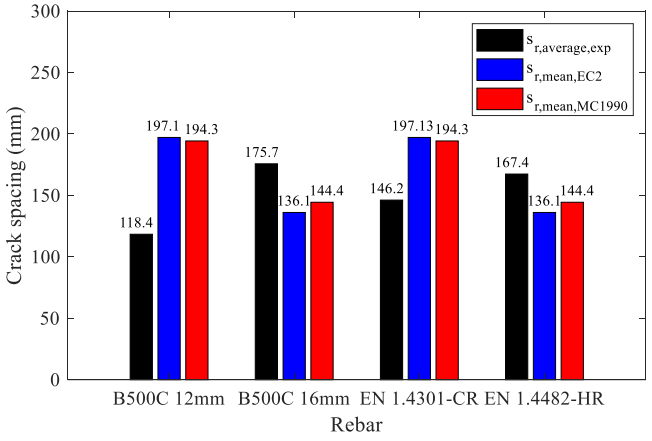

Fig. 15. Comparisons of measured and predicted crack spacings.

term loading, with all other parameters are as previously defined. Finally, the last stage of all three models, corresponding to the post-yield of the rebar, is modelled as a horizontal line with stress equal to the rebar yield stress f_y.

$$\varepsilon_m = (1-\zeta)\varepsilon_1 + \zeta\varepsilon_2 \quad \text{for} \quad \sigma_{cr} < \sigma \leq f_y \tag{9}$$

Table 12
Measured mean crack width vs. predicted mean crack widths from *Eurocode 2* at stress = 0.8 f_y.

	B500C 12 mm		B500C 16 mm		EN 1.4301-CR		EN 1.4482-HR	
	Test	EC2	Test	EC2	Test	EC2	Test	EC2
Test 1	0.40	**0.31**	0.40	**0.28**	0.56	**0.37**	0.55	**0.27**
Test 2	0.32		0.57		0.39		0.49	
Test 3	0.37		0.60		0.69		0.56	
Average	**0.36**		**0.52**		**0.55**		**0.53**	

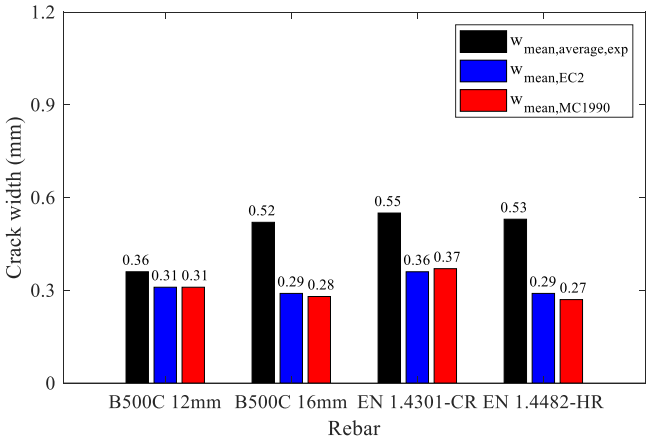

Fig. 16. Comparison of average measured mean crack width and predicted mean crack width.

Table 11
Measured mean crack width vs. predicted mean crack widths from *Model Code 1990* at stress = 0.8 f_y.

	B500C 12 mm		B500C 16 mm		EN 1.4301-CR		EN 1.4482-HR	
	Test	MC1990	Test	MC1990	Test	MC1990	Test	MC1990
Test 1	0.40	**0.31**	0.40	**0.29**	0.56	**0.36**	0.55	**0.29**
Test 2	0.32		0.57		0.39		0.49	
Test 3	0.37		0.60		0.69		0.56	
Average	**0.36**		**0.52**		**0.55**		**0.53**	

Table 13
Measured maximum crack width vs. predicted maximum crack widths from *Model Code 1990* at stress = 0.8 f_y.

	B500C 12 mm		B500C 16 mm		EN 1.4301-CR		EN 1.4482-HR	
	Test	MC1990	Test	MC1990	Test	MC1990	Test	MC1990
Test 1	0.40	**0.46**	0.45	**0.44**	0.84	**0.55**	0.57	**0.43**
Test 2	0.35		0.78		0.44		0.58	
Test 3	0.55		0.80		0.75		0.62	
Average	**0.43**		**0.68**		**0.68**		**0.59**	

Table 14
Measured maximum crack width vs. predicted maximum crack widths from *Model Code 2010* at stress = 0.8 f_y.

	B500C 12 mm		B500C 16 mm		EN 1.4301-CR		EN 1.4482-HR	
	Test	MC2010	Test	MC2010	Test	MC2010	Test	MC2010
Test 1	0.40	**0.60**	0.45	**0.61**	0.84	**0.71**	0.57	**0.59**
Test 2	0.35		0.78		0.44		0.58	
Test 3	0.55		0.80		0.75		0.62	
Average	**0.43**		**0.68**		**0.68**		**0.59**	

Table 15
Measured maximum crack width vs. predicted maximum crack widths from *Eurocode 2* at stress = 0.8 f_y.

	B500C 12 mm		B500C 16 mm		EN 1.4301-CR		EN 1.4482-HR	
	Test	EC2	Test	EC2	Test	EC2	Test	EC2
Test 1	0.40	**0.53**	0.45	**0.47**	0.84	**0.63**	0.57	**0.46**
Test 2	0.35		0.78		0.44		0.58	
Test 3	0.55		0.80		0.75		0.62	
Average	**0.43**		**0.68**		**0.68**		**0.59**	

$$\zeta = 1 - \beta_1 \left(\frac{\sigma_{cr}}{\sigma}\right)^2 \tag{10}$$

4.1.2. Comparison of tension stiffening responses with codified models

Comparisons between the predicted cracking stress $\sigma_{cr,pred}$, obtained from Eq. (4), and the experimental cracking stress $\sigma_{cr,exp}$, taken as the average value of the three repeat tests per specimen, are presented in Fig. 12. In all cases, the predicted cracking stresses were higher than the experimental values by 37 %-78 %, as has been observed in similar literature studies [28]. This discrepancy arises because the predicted cracking stresses are based on assumptions of elastic behaviour and perfect bond conditions, whereas in the experiments, bond imperfections or pre-existing microcracks may be present before full cracking occurs. Furthermore, the actual tensile strength of the concrete in this study may be lower than measured, as indirect testing methods – such as splitting and flexural tests – are known to overestimate tensile strength relative to direct tension testing [20].

Due to the discrepancy between the predicted and measured cracking stresses, the experimentally measured mean cracking stress values were used, similar to [28], to assess the analytical models' ability to quantify the tension stiffening effect without the influence of overestimated cracking stress, as shown in Fig. 13. To evaluate the accuracy of the assessed models quantitatively, the dissipated energy, taken as the area under the tension stiffening stress-strain curve, up to the yield stress of the bare rebar (reported in Table 4), was calculated for both the measured and predicted responses. The results are presented in Table 9. For both 12 mm and 16 mm diameter B500C carbon steel rebars, all assessed codified models generally show good agreement with the measured responses, with the *Eurocode 2* model providing the closest agreement. For the stainless steel rebars, all codified models overpredict the tension stiffening response, particularly for the 12 mm EN 1.4301-CR specimens, as they are unable to capture the inherent nonlinearity of stainless steel behaviour.

4.1.3. Modified tension stiffening model for stainless steel reinforcing bars

The tension stiffening models were modified to represent the behaviour of stainless steel rebars more accurately. The proposed modifications are based on adopting the two-stage Ramberg-Osgood model to describe the stress-strain behaviour of the bare rebar. The Ramberg-Osgood model, given in Eq. (11), is commonly used to model the nonlinear stress-strain behaviour of stainless steel [23,24] and is

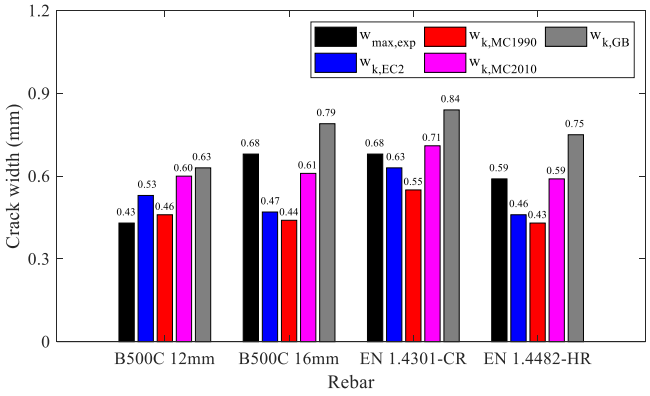

Fig. 17. Comparison of average measured maximum crack width and predicted maximum crack width.

Table 16
Measured maximum crack width vs. predicted maximum crack widths from *GB50010* at stress = 0.8 f_y.

	B500C 12 mm		B500C 16 mm		EN 1.4301-CR		EN 1.4482-HR	
	Test	GB50010	Test	GB50010	Test	GB50010	Test	GB50010
Test 1	0.40	**0.63**	0.45	**0.79**	0.84	**0.84**	0.57	**0.75**
Test 2	0.35		0.78		0.44		0.58	
Test 3	0.55		0.80		0.75		0.62	
Average	**0.43**		**0.68**		**0.68**		**0.59**	

recommended in British Standard 6744 [29] for stainless steel rebars. Based on the adoption of the Ramberg-Osgood model, the resulting modifications to each tension stiffening model are as follows:

- *Model Code 1990*: Eqs. (5) and (6) are used together with (i) the strain of the bare rebar, ε_2 (strain in the fully cracked state), obtained from Eq. (11), and (ii) the steel strain at the first crack, $\varepsilon_{sr,2}$, obtained from Eq. (12).
- *Model Code 2010*: Eqs. (7) and (8) are used together with the strain of the bare rebar, ε_2, obtained from Eq. (11).
- *Eurocode 2*: Eqs. (9) and (10) are used together with the strain of the bare rebar, ε_2, obtained from Eq. (11).
- All three models: The yield stress plateau for stresses beyond the yield stress is removed and replaced with a continuation of the previous stage of the stress–strain response, as described above.

$$\varepsilon_2 = \begin{cases} \dfrac{\sigma}{E} + 0.002\left(\dfrac{\sigma}{f_y}\right)^n, & \sigma \le f_y \\ \dfrac{\sigma - f_y}{E_{0.2}} + \left(\varepsilon_u - \varepsilon_{t,0.2} - \dfrac{f_u - f_y}{E_{0.2}}\right)\left(\dfrac{\sigma - f_y}{f_u - f_y}\right)^{n'} + \varepsilon_{t,0.2}, & \sigma > f_y \end{cases} \tag{11}$$

$$\varepsilon_{sr,2} = \frac{\sigma}{E} + 0.002\left(\frac{\sigma_{cr}}{f_y}\right)^n \tag{12}$$

where, $E_{0.2}$ is the tangent modulus at 0.2 % proof stress ($E_{0.2} = E/(1 + (0.002nE/f_y))$), $\varepsilon_{t,0.2}$ is the total strain at 0.2 % proof stress ($\varepsilon_{t,0.2} = f_y/E + 0.002$) and all other variables are defined in Section 3.1.

Comparisons of the modified *Eurocode 2*, *Model Code 1990* and *Model Code 2010* tension stiffening models with the test responses are shown in Fig. 14. The corresponding dissipated energy values, again taken as the area under the tension stiffening stress-strain curve up to yield stress of the bare rebar (reported in Table 4), are presented in Table 10. The modified models demonstrate good agreement with the measured responses, capturing both the nonlinear post-cracking tension stiffening behaviour and the post-yield tension stiffening of the stainless steel rebars.

4.2. Assessment of codified crack spacing and width models

4.2.1. Overview of codified crack spacing and crack width recommendations

Standards such as *Model Code 1990*, *Model Code 2010*, *Eurocode 2* and *GB50*010*–2010* [30] provide guidance on the maximum allowable crack width for reinforced concrete structural elements, considering both durability and appearance, and are dependent on exposure classification. These standards also provide methods for predicting the mean crack width w_{mean}, characteristic crack width w_k and crack spacing s_r in reinforced concrete members. The characteristic crack width w_k represents the 95th percentile of crack widths and is often used interchangeably with the maximum crack width in literature [31].

Model Code 1990 defines the maximum crack spacing, $s_{r,max}$, as twice the transmission length, $l_{s,max}$, according to Eq. (13). *Model Code 2010* defines $s_{r,max}$ similarly, but also includes the concrete cover, c, multiplied by a correction factor k (taken as 1), as given in Eq. (14). In the calculation of $s_{r,max}$, both *Model Code 1990* and *Model Code 2010* assume the bond stress τ_{bm} to be equal to the tensile stress of concrete f_t multiplied by a factor of 1.8 for short-term loading. Moreover, in *Model Code 1990* $s_{r,mean,MC1990}$ is calculated as the product of the maximum crack spacing $s_{r,max}$ and a factor of 2/3, as shown in Eq. (15).

$$s_{r,max} = 2\left(\frac{f_t}{4\tau_{bm}}\frac{\varnothing}{\rho_s}\right) \tag{13}$$

$$s_{r,max} = 2\left(kc + \frac{f_t}{4\tau_{bm}}\frac{\varnothing}{\rho_s}\right) \tag{14}$$

$$s_{r,mean,MC1990} = \frac{2}{3}s_{r,max} = \frac{4}{3}l_{s,max} \tag{15}$$

In *Eurocode 2*, the mean crack spacing $s_{r,mean,EC2}$ is calculated using Eq. (16), which is a function of the clear concrete cover c_{clear}, the loading coefficient k_{fr}, the bonding conditions coefficient k_b, the rebar diameter $\varnothing$ and the reinforcement ratio ρ_s. *Eurocode 2* has a further requirement that the mean crack spacing does not exceed the difference between the section's height h and neutral axis x multiplied by a factor of $1.3/k_w$, where k_w is a conversion factor. When comparing with the experimental results, the loading coefficient k_{fr} was set to 1 for pure tension and k_b was set to 0.9 for good bond conditions. The limit on the mean crack spacing was not applied since the specimens were subjected to pure tension.

$$s_{r,mean,EC2} = 1.5c_{clear} + \frac{k_{fr}k_b}{7.2}\frac{\varnothing}{\rho_s} \tag{16}$$

In *Model Code 1990*, w_{mean} and w_k are calculated using Eqs. (17) and (18), respectively. These relationships are derived from crack spacing and the difference between the mean strain of steel reinforcement ε_{sm} and the mean strain of concrete between cracks ε_{cm}. Eq. (17) employs the mean crack spacing $s_{r,mean}$, i.e., the average distance between cracks along the length of a concrete element, while Eq. (18) uses the maximum crack spacing $s_{r,max}$, i.e., the largest distance between two consecutive cracks along a concrete member. *Model Code 2010* retains the same formulation as *Model Code 1990* for w_k (Eq. (18)) but does not provide a method for calculating w_{mean}.

$$w_{mean} = s_{r,mean}(\varepsilon_{sm} - \varepsilon_{cm}) \tag{17}$$

$$w_k = s_{r,max}(\varepsilon_{sm} - \varepsilon_{cm}) \tag{18}$$

The calculation of w_{mean} in *Eurocode 2* is similar to that *in Model Code 1990*, but includes an additional coefficient $k_{1/r}$ to account for the increase in crack width due to curvature. However, since the tension stiffening specimens in this study were subjected to pure tensile axial load, the $k_{1/r}$ coefficient is set to 1 [32], and therefore, the *Eurocode 2* relationship reduces to the *Model Code 1990* expression in Eq. (17). The characteristic crack width w_k in *Eurocode 2* is calculated using Eq. (19), where w_{mean} is multiplied by a conversion factor k_w, which is given a value of 1.7.

$$w_k = k_w k_{1/r} w_{mean} \tag{19}$$

The difference between the mean strain of steel reinforcement and the mean strain of concrete between cracks ($\varepsilon_{sm} - \varepsilon_{cm}$), is obtained from Eq. (20) in *Model Code 1990*, *Model Code 2010* and *Eurocode 2*. In Eq. (20), k_t is a coefficient that depends on the duration and nature of the loading and all other parameters are as previously defined. For the tests conducted in this study, a value of 0.6 was assigned to k_t for short term loading. In addition, *Eurocode 2* applies an additional condition to Eq. (20), where ($\varepsilon_{sm} - \varepsilon_{cm}$) must be greater or equal to $(1 - k_t)\sigma/E$. Furthermore, considering Eq. (4) for the definition of σ_{cr}, Eq. (20) can be simplified to Eq. (21), where the value of σ_{cr} was set to the measured cracking stress $\sigma_{cr,exp}$, as discussed in Section 4.1.2.

$$(\varepsilon_{sm} - \varepsilon_{cm}) = \frac{\sigma}{E} - k_t\frac{f_t(1 + \alpha_s\rho_s)}{\rho_s E} \tag{20}$$

$$(\varepsilon_{sm} - \varepsilon_{cm}) = \frac{\sigma}{E} - k_t\frac{\sigma_{cr}}{E} \tag{21}$$

The characteristic crack width w_k according to the Chinese code *GB50010–2010* is obtained using the expression in Eq. (22), where α_{cr} is the component load characteristic coefficient, which for tension is given a value of 2.7, ψ is a coefficient for strain of tensile reinforcement between cracks (Eq. (23)) and all other parameters are as previously

defined.

$$w_k = \alpha_{cr}\varphi\frac{\sigma}{E}\left(1.9c + 0.08\frac{\varnothing}{\rho_s}\right) \quad (22)$$

$$\varphi = 1.1 - 0.65\frac{f_t}{\rho_s\sigma} \quad (23)$$

4.2.2. Evaluation of codified mean crack spacing

The measured average crack spacings $s_{r,average,exp}$ reported in Table 6 were compared with the predicted mean crack spacings from *Model Code 1990* $s_{r,mean,MC1990}$ and *Eurocode 2* $s_{r,mean,EC2}$, as shown in Fig. 15. The mean crack spacing calculated using *Model Code 1990* overestimated the experimentally measured average crack spacings for specimens with 12 mm diameter rebars, while underestimating it for specimens with 16 mm diameter rebars. These discrepancies can be attributed to the assumed bond strength of 1.8 f_t, which appears to be conservative for 12 mm rebars but unconservative for 16 mm rebars. The *Eurocode 2* mean crack spacing approach exhibited similar trends to the *Model Code 1990* but provided slightly less accurate estimates of the measured mean crack spacings.

4.2.3. Evaluation of codified mean and characteristic crack widths

The measured crack widths were compared with the crack widths predicted by design codes. The measured mean crack widths for each specimens $w_{mean,exp}$ defined as the average of the crack widths across multiple cracks in a given specimen at stress equal to 0.8f_y, which is typically taken as the serviceability limit stress in steel reinforcing bars, and the predicted mean crack width at the same stress level based on *Model Code 1990* $w_{mean,MC1990}$ and *Eurocode 2* $w_{mean,EC2}$ are presented in Tables 11 and 12, respectively. Fig. 16 further illustrates the comparison between the average measured mean crack widths and the predicted values from *Model Code 1990* and *Eurocode 2*. As shown in Fig. 16, both codes consistently underestimate the measured crack widths for all specimens. However, this underestimation is less pronounced for the B500C 12 mm rebars, where $w_{mean,MC1990}$ and $w_{mean,EC2}$ are 13.9 % lower than the measured value, compared to underpredictions ranging from 32.7 % to 49.1 % for the other tested rebars. Both codes yield similar predictions since they employ the same formulation (Eq. (17)), with only minor discrepancies arising from small differences in the calculated mean crack spacings.

Since the characteristic crack width is considered comparable to the experimentally measured maximum crack widths, these values were also compared. The measured maximum crack widths for each specimen $w_{max,exp}$ taken as the maximum crack widths across multiple cracks in a given specimen at stress equal to the rebar 0.8f_y, and the predicted characteristic crack width, based on *Model Code 1990* $w_{k,MC1990}$, *Model Code 2010* $w_{k,MC2010}$, *Eurocode 2* $w_{k,EC2}$ and *GB50010* $w_{k,GB}$ are presented in Tables 13, 14, 15 and 16, respectively. Fig. 17 further illustrates the comparison between the average measured maximum crack widths and the predicted characteristic values. Fig. 17 shows that for the B500C 12 mm rebar, $w_{k,MC1990}$ provided very good agreement with the experiments, overestimating $w_{max,exp}$ by only 6.5 %, whereas $w_{k,MC2010}$, $w_{k,EC2}$ and $w_{k,GB}$ resulted in larger overestimations of 38.6 %, 22.4 %, and 47.4 %, respectively. For B500C 16 mm rebars, $w_{k,MC1990}$ and $w_{k,EC2}$ underestimated $w_{max,exp}$ by 35.2 % and 30.8 %, respectively, while $w_{k,MC2010}$ showed better agreement with a 10.1 % underestimation and $w_{k,GB}$ again overestimated by 16.7 %. For stainless steel rebars, *Eurocode 2* and *Model Code 1990* generally underestimated $w_{max,exp}$ by 7.4–27.4 %, whereas *Model Code 2010* and *GB50010* typically overestimated it by 0.7–27 %.

5. Concluding remarks

This study investigated the tension stiffening behaviour of stainless steel rebars through experimental testing of 12 mm cold-rolled austenitic EN 1.4301-CR and 16 mm hot-rolled lean-duplex EN 1.4482-HR stainless steel rebars, alongside carbon steel B500C rebars for comparison. The measured tension stiffening responses and crack behaviours were presented and discussed. The codified guidelines in terms of the tension-stiffening stress-strain models, mean crack spacing and crack width models from *Eurocode 2, Model Code 1990* and *Model Code 2010* were also assessed. This study is the first to investigate the tension stiffening behaviour of ribbed stainless steel rebars using direct tension tests. The findings provide new insights into how stainless steel differs from carbon steel reinforcement and have practical implications for serviceability design, particularly through the adoption of the Ramberg–Osgood model for stainless steel rebars. The key findings are as follows:

- Tension stiffening trends were similar for stainless and carbon steel up to the first crack, but differences emerged due to stainless steels nonlinear stress-strain behaviour.
- The tension stiffening effect was less pronounced in specimens containing 12 mm stainless steel rebars compared with 12 mm carbon steel rebars but was similar in specimens with 16 mm stainless steel rebars and carbon steel rebars.
- Tension stiffening persisted beyond the 0.2 % proof stress for stainless steel rebars, before gradually decaying towards the bare rebars tensile response, which could potentially affect stainless steel reinforced concrete members deflections and crack widths, warranting further investigation.
- The measured average crack spacing was larger for specimens containing cold-rolled EN 1.4301 12 mm stainless steel rebars due to the poorer bond strength of such rebars compared with carbon steel rebars, while 16 mm rebars had similar crack spacing across rebar materials. Stainless steel reinforced specimens exhibited larger measured crack widths at yield but significantly smaller post-yield crack widths, highlighting the potential of stainless steel rebars for limiting crack growth in reinforced concrete structures.
- Codified tension stiffening models commonly used were compared with the experimental results. The models were shown to generally be in good agreement with the carbon steel rebar tension stiffening specimen experimental responses during the crack stabilisation stage, while for the stainless steel rebar tension stiffening specimens, the models were not capable of accurately capturing the nonlinear effects of the material. Modifications to the codified tension stiffening models, incorporating the nonlinear two-stage Ramberg-Osgood model, were suggested and demonstrated improved agreement with stainless steel rebar tension stiffening behaviour.
- *Model Code 1990* and *Eurocode 2* overestimated crack spacing for 12 mm rebars but underestimated it for 16 mm rebars. Both models underpredicted the measured mean crack widths. For maximum crack width, *Model Code 1990* gave the best agreement with the 12 mm carbon steel rebars, while *Model Code 2010* provided the closest predictions for the other rebar types.
- Future work should build upon the present study by conducting direct tension tests on stainless steel specimens to investigate the influence of creep and shrinkage on tension stiffening behaviour. In addition, beam tests are recommended to account for the combined effects of bending, shear and axial forces, and to further validate the findings on crack width and spacing.

Declaration of Competing Interest

As the corresponding author of the above-named manuscript, and on behalf of my co-authors, I wish to confirm that there are no known conflicts of interest associated with this publication and there has been no significant financial support for this work that could have influenced its outcome.

Data availability

Data will be made available on request.

References

[1] Mak MWT, Desnerck P, Lees JM. Corrosion-induced cracking and bond strength in reinforced concrete. Constr Build Mater 2019;208:228–41.
[2] Markeset G, Rostam S, Klinghoffer O. Guide for the Use of Stainless Steel Reinforcement in Concrete Structures. Norwegion Building Research Institute.; 2006.
[3] Moodley H, Afshan S, Blainey S, Preston J. State-of-the-art review on the structural behaviour of stainless steel reinforced concrete elements'. 11th Int Conf Bridge Maint Saf Manag 2022.
[4] Gardner L, Bu Y, Francis P, Baddoo NR, Cashell KA, McCann F. Elevated temperature material properties of stainless steel reinforcing bar. Constr Build Mater 2016;114:977–97.
[5] Zhou Y, Uy B, Wang J, Li D, Huang Z, Liu X. Behaviour and design of stainless steel-concrete composite beams'. J Constr Steel Res 2021;185:106863.
[6] Melo J, Afshan S, Rossetto T, Varum Y, Arêde A. Experimental and numerical investigation of the cyclic response of stainless steel reinforced concrete columns. Eng Struct 2021;252.
[7] Moodley H, Blainey S, Preston J, Afshan S. Can stainless steel reinforcement bar facilitate more sustainable railway bridges? A comparative life cycle cost and carbon analysis'. World Congr Railw Res Birm 2022.
[8] Albitar M, Mohamed Ali MS, Visintin P. Evaluation of tension-stiffening, crack spacing and crack width of geopolymer concretes. Constr Build Mater 2018;160:408–14.
[9] Yu Y, Zhou L, Liao Z, Zheng Y. Tension stiffening and cracking behaviors in glass fiber reinforced polymer bar enhanced precast recycled aggregate concrete specimen'. Structures 2024;69:107395.
[10] Moodley H, Afshan S, De Risi R. Low-cycle fatigue behaviour and strain-life model of stainless steel reinforcing bars'. Structures 2024;67:106994.
[11] Limbert J, Afshan S, Kashani MM, Robinson AF. Compressive stress–strain behaviour of stainless steel reinforcing bars with the effect of inelastic buckling. Eng Struct 2021;237.
[12] Moodley H, Afshan S, Crump D, Kashani MM. Testing and numerical modelling of circular stainless steel reinforced concrete columns'. Eng Struct 2024;304:117607.
[13] CEN. EN 1992-1-1 Eurocode 2: Design of Concrete Structures. Part 1-1: General Rules and Rules for Buildings, Bridges and Civil Engineering Structures. Brussels: European Committee for Standardization; 2023.
[14] CEB-FIP. Model Code 1990 - Design Code. Switzerland: The International Federation for Structural Concrete; 1993.
[15] fib. Model Code 2010 - First Complete Draft. Fib Bulletin 56. Switzerland: The International Federation for Structural Concrete; 2010.
[16] Tinevez J-Y, et al. TrackMate: an open and extensible platform for single-particle tracking. Methods 2017;115:80–90.
[17] Schneider CA, Rasband WS, Eliceiri KW. NIH image to ImageJ: 25 years of image analysis. Nat Methods 2012;9(7):671–5.
[18] CEN. EN ISO 6892-1: Metallic Materials. Tensile Testing. Method of Test at Room Temperature. Brussels: European Committee for Standardization; 2019.
[19] CEN. EN 12390-3: Testing Hardened Concrete. Compressive Strength of Test Specimens. Brussels: European Committee for Standardization; 2019.
[20] ASTM. ASTM C496/C496M-04: Standard Test Method for Splitting Tensile Strength of Cylindrical Concrete Specimens. West Conshohocken: ASTM International; 2004.
[21] ASTM. ASTM C78/C78M-18: Standard Test Method for Flexural Strength of Concrete (Using Simple Beam with Third-Point Loading). West Conshohocken: ASTM International; 2018.
[22] Hung C-C, Lee H-S, Chan SN. Tension-stiffening effect in steel-reinforced UHPC composites: constitutive model and effects of steel fibers, loading patterns, and rebar sizes. ' Compos B Eng 2019;158:269–78.
[23] Mirambell E, Real E. On the calculation of deflections in structuralstainless steel beams: an experimental andnumerical investigation. J Constr Steel Res 2000;54:109–33.
[24] Rasmussen KJR. Full-range stress–strain curves for stainless steel alloys. J Constr Steel Res 2003;59:47–61.
[25] Afshan S, Rossi B, Gardner L. Strength enhancements in cold-formed structural sections — part I: material testing. J Constr Steel Res 2013;83:177–88.
[26] R. L'Hermite, Idées actuelles sur la technologie du béton [Current ideas on concrete technology]. Documentation technique du bâtiment et des travaux publics, 1955. [Online]. Available: ⟨https://books.google.co.uk/books?id=dHZkAAAAMAAJ⟩.
[27] Rabi M, Cashell KA, Shamass R, Desnerck P. Bond behaviour of austenitic stainless steel reinforced concrete. Eng Struct 2020;221.
[28] Gaztelumendi DE. Bond Behaviour and Tension Stiffening of Flat Stainless Steel Rebars with Continuous or Alternate Rib Pattern Embedded in Concrete. Ghent: Ghent University; 2012.
[29] BSI. BS 6744:2023 Stainless Steel Bars. Reinforcement of Concrete. Requirements and Test Methods. British Standards Institute; 2023.
[30] The Ministry of Housing and Urban-Rural Construction of the People's Republic of China, *GB50010-2010, Code for the Design of Concrete Structures*. Beijing, 2010.
[31] Lapi M, Orlando M, Spinelli P. A review of literature and code formulations for cracking in R/C members'. Struct Concr 2018;19(5):1481–503.
[32] Van Der Esch A, Wolfs R, Fennis S, Roosen M, Wijte S. Categorization of formulas for calculation of crack width and spacing in reinforced concrete elements. Struct Concr 2024;25(1):32–48.